

Rashba interaction and local magnetic moments in a graphene-Boron Nitride heterostructure by intercalation with Au

E.C.T. O'Farrell,^{*} J.Y. Tan, Y. Yeo, G.K.W. Koon, and B. Özyilmaz[†]

Centre for Advanced 2D Materials and Graphene Research Centre,

National University of Singapore, 117546, Singapore. and

Department of Physics, National University of Singapore, 117542, Singapore.

K. Watanabe and T. Taniguchi

National Institute for Materials Science, 1-1 Namiki, Tsukuba 305-0044, Japan.

We intercalate a van der Waals heterostructure of graphene and hexagonal Boron Nitride with Au, by encapsulation, and show that Au at the interface is two dimensional. A charge transfer upon current annealing indicates redistribution of Au and induces splitting of the graphene bandstructure. The effect of in plane magnetic field confirms that splitting is due to spin-splitting and that spin polarization is in the plane, characteristic of a Rashba interaction with magnitude approximately 25 meV. Consistent with the presence of intrinsic interfacial electric field we show that the splitting can be enhanced by an applied displacement field in dual gated samples. Giant negative magnetoresistance, up to 75%, and a field induced anomalous Hall effect at magnetic fields < 1 T are observed. These demonstrate that hybridized Au has a magnetic moment and suggests the proximity to formation of a collective magnetic phase. These effects persist close to room temperature.

Spin orbit coupling in graphene is induced by hybridization with heavy metals [1]. This has been achieved by intercalation of graphene using e.g. Au, which produces a Rashba interaction ~ 100 meV [2], and Pb [3], on metallic substrates. We intercalate Au into a heterostructure of graphene and dielectric hexagonal Boron Nitride (*h*BN), and report spin-splitting of the graphene bands observed in quantum oscillations on an insulating substrate, a crucial requirement for applications. The Rashba interaction is large (25 meV) for samples intercalated with 0.1 monolayers (ML) of Au, but is modulated by modest electric fields, thereby highlighting the requirement of hybridization with spin-split Au *d*-electrons [2]. We observe large negative magnetoresistance, up to 75%, indicating Au ions form magnetic moments and an anomalous Hall effect suggests the possible formation of a collective magnetic phase. The combination of Rashba interaction, magnetic moments and electric field control of the density, is akin to dilute magnetic semiconductors [4], and in a Dirac material opens a route toward electric field control of magnetism and engineering topological magnetic states such as the quantum anomalous Hall effect [5, 6].

The van der Waals interaction can create an atomically clean interface between stacked two-dimensional (2D) crystals [7]; therefore, it can be considered organizing principle for atoms or molecules at a hetero-interface [8]. Here, we use the van der Waals interaction to cleanly intercalate Au between graphene and *h*BN and to induce strong hybridization between graphene and Au. We intercalate graphene-*h*BN heterostructures by depositing 0.1-0.5 nominal ML of Au onto freshly cleaved *h*BN on SiO₂ in ultra high vacuum. Au decorated *h*BN is used as the substrate onto which a separately prepared graphene/*h*BN (thickness ≈ 20 nm) is transferred, the structure is illustrated in Fig. 1a. The stack is etched and metallic contacts are formed at the exposed edges of graphene [9]. Following thermal annealing the heterostructure is flat with root mean square roughness of 0.16 nm (Fig. 1b and c)

over lateral regions of several micron, this demonstrates the absence of 3D clusters of Au at the graphene/*h*BN interface (see supplementary information for additional information on cluster formation and Au motion). We fabricate the device in these flat regions where Raman spectroscopy measurements show the absence of bulk strain (supplementary information).

The interaction of Au and graphene has been extensively studied both by photoemission and transport. Graphene on SiC intercalated with Au shows large shifts in doping ($> 10^{13}$ cm⁻²) depending on partial or full intercalation [10], whereas graphene intercalated on Ni remains close to the neutrality point [2]. In transport measurements on SiO₂ quasi-continuous Au-film growth on graphene induces weak *p*-doping of -5×10^{11} cm⁻², consistent with the lower vacuum level of bulk Au. However, Au in a nanoparticle configuration [11] induces *n*-doping $+5 \times 10^{11}$ cm⁻² attributed to the reduced Au-graphene separation and lower effective potential. Clustered Au produces local variations in the Fermi level and scattering leading to positive linear MR [12] and an extrinsic spin Hall effect [13, 14].

Au is always present in the samples presented here, but as fabricated samples show longitudinal (ρ_{xx}) and Hall (ρ_{xy}) resistivity characteristic of pristine graphene, shown in Fig. 1d for 0.1 ML Au and field effect mobility 1.2×10^5 cm²/Vs; however, the MR is negative (supplementary information). We observe Au at the interface is mobile even at room temperature (supplementary information), this suggests isolated Au will gather into 2D clusters. To achieve the uniform Au distribution which is our goal we perform a low temperature current anneal that redistributes and then quenches the Au configuration. Low temperature post-growth annealing is typical in the synthesis of dilute magnetic semiconductors, to evenly distribute magnetic ions [15, 16].

Current annealing (see supplementary information) induces diffusive migration of Au on graphene [17]. This shifts the charge neutrality point by $\delta V_{bg} = -8.4$ V making graphene

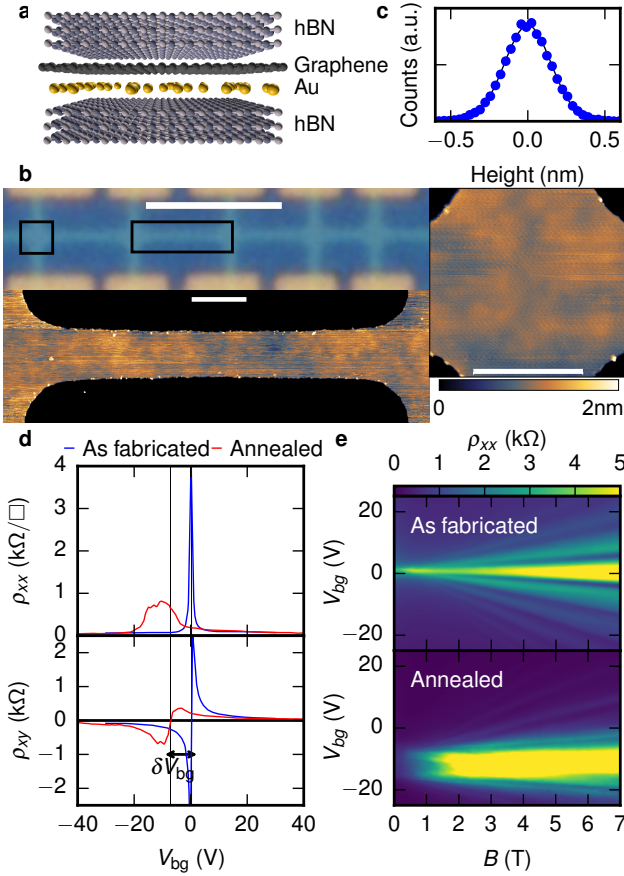


FIG. 1. **a**, Schematic of the Au intercalated graphene-hBN heterostructure. **b**, optical (upper left, scale bar $5\ \mu\text{m}$) and atomic force micrographs (scale bars $0.5\ \mu\text{m}$) of a fully encapsulated and etched device, black boxes indicate regions in the atomic force micrographs. **c**, height histogram of a $1\ \mu\text{m}^2$ area of the device channel, fit to a Gaussian with roughness = $0.16\ \text{nm}$. **d**, ρ_{xx} and ρ_{xy} against V_{bg} at $T = 1.2\ \text{K}$ and $B = 0$ and $0.2\ \text{T}$, respectively, for a $0.1\ \text{ML}$ intercalated device, both as fabricated and after current annealing. **e**, as fabricated and after current annealing ρ_{xx} against V_{bg} and B , at $T = 1.2\ \text{K}$ for a $0.1\ \text{ML}$ intercalation.

electron doped (Fig. 1d), the doping is $e\delta n_e = C_{\text{bg}}\delta V_{\text{CNP}}$, where C_g is the gate capacitance and e is the electron charge, giving $\approx 5 \times 10^{11}\ \text{cm}^{-2}$. Following previous studies we infer further n -doping is due to a less clustered, more uniform distribution. After annealing the application of magnetic field B shows that the Landau levels (LLs) are split (Fig. 1e). We note that the mobility of Au will lead to the loss of some Au from the channel so the final concentration is less than deposition.

Figure 2a shows the ρ_{xx} against V_{bg} under various B_{\perp} . LL formation is visible, but, integer quantum Hall effect plateaus are visible only in ρ_{xy} . This is comparable to the case of tri-layer graphene which has both linear and quadratically dispersing bands leading to a residual density of states [18].

To resolve features in the electronic structure we take the derivative $d\rho_{xx}/dV_{\text{bg}}$ (Fig. 2b). At positive V_{bg} well defined LLs are clearly seen as part of a Landau fan from

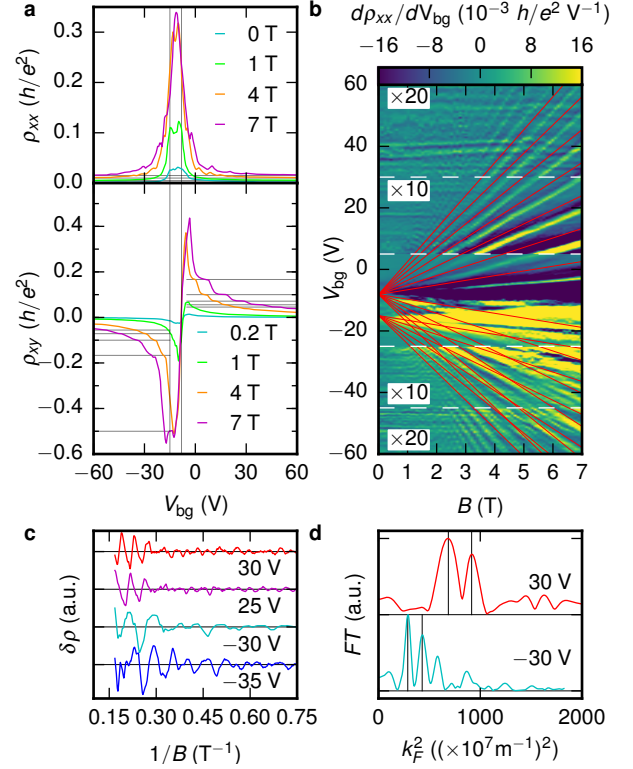


FIG. 2. **a**, ρ_{xx} and ρ_{xy} against V_{bg} for a $0.1\ \text{ML}$ intercalated device at $T = 1.2\ \text{K}$, for various B_{\perp} (ρ_{xx} shifted by $0.01\ h/e^2$ for clarity). **b**, derivative $d\rho_{xx}/dV_{\text{bg}}$ against V_{bg} and B_{\perp} , overlaid with Landau fan as guide to the eye. Regions at positive and negative V_{bg} are magnified as indicated. **c**, oscillatory part of the MR against $1/B$ for various V_{bg} . **d**, Fourier transform of the MR with first harmonic peaks indicated.

$V_{\text{bg}} = -8.15\ \text{V}$. At positive V_{bg} we show a Landau fan for LLs with $N = \dots, 2, 4, 10, \dots$ as a guide to the eye, corresponding to the valley degeneracy of graphene. At negative V_{bg} LL clearly emerge from a second Landau fan displaced by $\delta V_{\text{bg}} = -6.5\ \text{V}$. This second fan has a pronounced asymmetry, appearing more prominently in the valence band close to neutrality. This asymmetry is sensitive to the concentration of Au intercalation, for $0.5\ \text{ML}$ more pronounced splitting was observed in the conduction band (supplementary information). Non-dispersive features are observed e.g. at $V_{\text{bg}} \approx 40\ \text{V}$, these may arise from damage to the contacts during annealing or extrinsic resonances [13]; however, these do not couple to the spin dependent transport reported later.

The splitting wavevector is extracted from quantum oscillations (Fig. 2c and d) in the valence and conduction band. Clear nodes in the oscillation are obscured by the presence of higher harmonic oscillations and anharmonicity. Anharmonicity may arise from spatial variations in the splitting due to variation in the Au distribution. We extract splittings $k_R = 3.8 \pm 0.2 \times 10^7$ and $4.0 \pm 0.2 \times 10^7\ \text{m}^{-1}$ in the valence and conduction bands respectively; yielding energy splittings 24 ± 2 and $26 \pm 2\ \text{meV}$, respectively, at $E_F > 100\ \text{meV}$ from neutrality, while split-

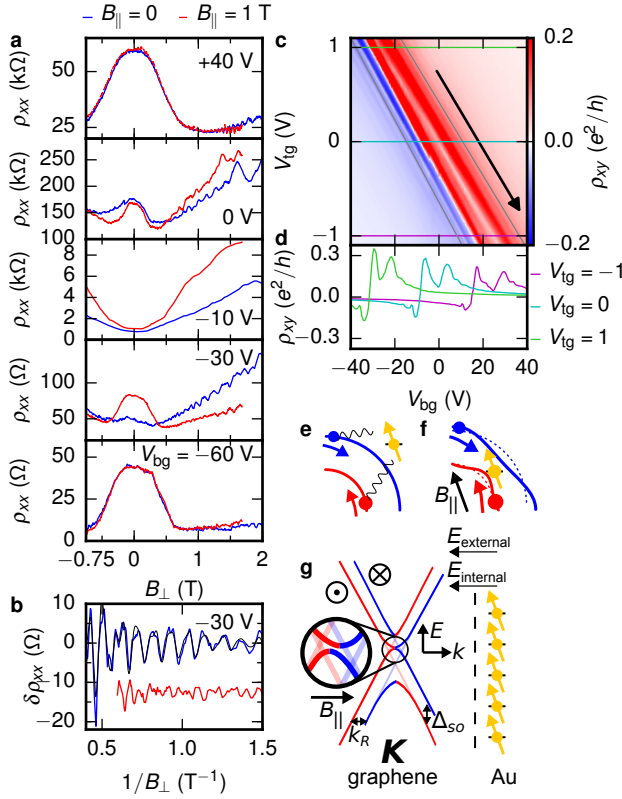


FIG. 3. **a**, ρ_{xx} against B_{\perp} at several V_{bg} , with and without $B_{||}$, at $T = 1.2$ K. **b**, Oscillatory component of ρ_{xx} for $V_{bg} = -30$ V from **a**. **c**, effect of external electric field on ρ_{xy} at $B = 2$ T, $T = 4.2$ K for a device with 0.5 ML intercalation. Gray lines indicate contours of constant density in valence and conduction bands, arrow indicates direction of increasing external electric field. **d**, cross-sections through **c**. **e** and **f**, Schematic illustration of scattering processes of spin-split electrons. **g**, Schematic bandstructure of graphene with Rashba interaction, spin circulation anti-clockwise and clockwise indicated as red and blue. Direction of inferred internal electric field $E_{internal}$ and applied $E_{external}$ indicated. Expanded region indicates effect of $B_{||}$.

ting is stronger on the valence band side closer to neutrality. We now show the splitting is spin splitting from a Rashba interaction.

Fig. 3a shows ρ_{xx} versus B_{\perp} at various V_{bg} (supplementary information for additional V_{bg}), with and without an additional in plane magnetic field $B_{||} = 1$ T. Far from neutrality there is negligible difference with and without $B_{||}$. Approaching neutrality $B_{||}$ alters the MR; negative MR is enhanced and the LL structure is significantly changed (Fig. 3b). In the split region, $-15 < V_{bg} < -8$ V, negative MR is absent and positive MR is enhanced.

The bandstructure of graphene with an Au induced Rashba interaction [2, 19] is illustrated schematically in Fig. 3g for the K valley, while spin polarizations are reversed in the K' valley. This identifies $-15 < V_{bg} < -8$ V as the regime where a single spin band is occupied in each valley. Negative MR is typical due to spin flip scattering between spin polarized

bands in materials with spin splitting, as illustrated schematically in Fig. 3e. Out of plane spin fluctuations are suppressed under applied B_{\perp} and cannot mediate inter-band scattering so resistance decreases. This is consistent with the results here showing negative MR is absent in the single band regime.

In plane magnetic will affect these local moments, but the change in the LL spectrum indicates instead changes in electronic structure. In plane magnetic field is known to alter the electronic structure in spin-split bands due to the effect of either finite quantum well width [20, 21] or the Zeeman interaction [22] as illustrated in Fig. 3f. These typically occur in relatively thick quantum wells or large fields and this behavior is surprising in graphene which is atomically thin and in pristine form has Landé g -factor ≈ 2 [23], so the Zeeman energy for $B_{||} = 1$ T is < 1 meV. We return to consider this point later.

Approaching the neutrality point from the valence band side negative MR decreases when $B_{||} = 0$ as the splitting wavevector increases. Negative MR is enhanced by the application of $B_{||}$, suggesting that $B_{||}$ decreases the separation of spin split bands in momentum space, illustrated in Fig. 3f. In the single band regime at -10 V the zero field resistance is not substantially changed but the MR is significantly larger under B_{\perp} for $B_{||} = 1$ T. The strong positive MR in the single band regime (Fig. 1e) may be the result of perpendicular Zeeman interaction inducing a gap in the spectrum [24], analogously to the exchange interaction [5]. This effect would be reduced by disorder but enhanced when the bands are displaced under $B_{||}$ as illustrated in the expansion.

We now consider the effect of an additional applied electric field in a second sample with Au concentration 0.5 ML and top and bottom gates enabling the application of a displacement field to the Au/graphene interface. For this sample splitting around the neutrality was found to be more strongly enhanced in the conduction band, but graphene is again electron doped by Au. ρ_{xy} at $B = 2$ T is shown in Fig. 3d at several top gate voltages.

Au hybridized with graphene ionizes, donating charge to graphene and inducing an electric field in the same direction. Even for the case of pristine graphene this electric field can induce spin splitting [25, 26]; however, this requires extremely large electric fields > 10 V/nm. Fig. 3c shows that applying an external electric field the splitting can be enhanced or reduced. When the external field is aligned with the internal field from Au to graphene (indicated by the arrow) splitting increases such that contours of constant in the hole and electron bands are driven apart, indicated by the gray lines. Assuming energy and V_{bg} are approximately linear in this narrow interval we observe 25% increase in the splitting for an external field of ≈ 0.5 V/nm $^{-1}$. The relatively large effect of this modest external electric field therefore indicates that spin orbit coupling is induced through spin dependent hybridization with the strong spin orbit coupled d -band of Au deep in the valence band of graphene [2].

We now consider the magnetic properties, Fig. 4a shows MR at various densities. At negative density sharp kinks are

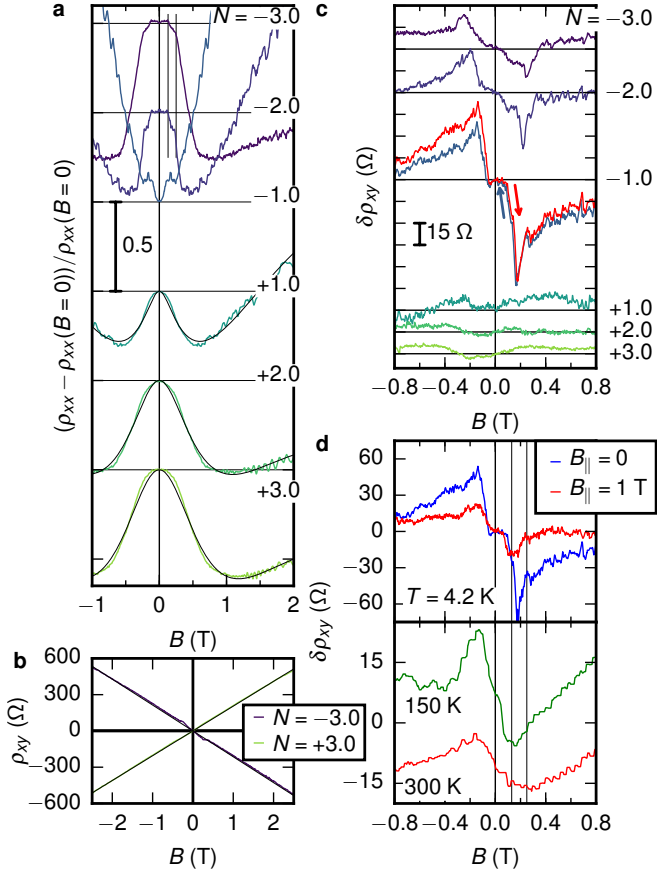


FIG. 4. Densities N are $\times 10^{12} \text{ cm}^{-2}$. **a**, Low field MR at various N , $T = 4.2 \text{ K}$, dashed lines are fits to Eqn. 1. **b**, ρ_{xy} at hole and electron densities, $T = 4.2 \text{ K}$. **c**, ρ_{xy} after subtracting a linear normal Hall effect component. **d** **upper panel**, Effect of $B_{||}$ on non-linear component of Hall effect at $N = -1 \times 10^{12} \text{ cm}^{-2}$. **Lower panel**, effect of temperature.

visible at $B = 0.11$ and 0.24 T , and the MR is up to 75%. The absence of hysteresis (supplementary information) at these fields indicates this is not a first order transition such as ferromagnetism. At positive density the MR is smooth and we fit the MR to the Khosla-Fischer expression for spin-flip scattering by local moments [27]:

$$\frac{\Delta\rho}{\rho_0} = -a^2 \ln(1 + b^2 H^2) + \frac{c^2 H^2}{1 + d^2 H^2} \quad (1)$$

$$a = A_1 J D(\epsilon_F) [S(S+1) + \langle M^2 \rangle]$$

$$b^2 = \left[1 + 4 S^2 \pi^2 \left(\frac{2 J D(\epsilon_F)}{g} \right)^4 \right] \left(\frac{g \mu_B}{\alpha k_B T} \right)^2.$$

The first term is due to local moment scattering and the second is the MR of a 2 band metal; a and b are functions of the magnetic exchange interaction J , the magnetization M , the local magnetic moment S , the density at the Fermi level $D(\epsilon_F)$. A_1 describes the contribution of spin scattering to the MR and α is a constant of assumed to be of order 1. Eqn. 1 fits well,

the MR increases at higher density (see supplementary information for parameters). This implies Au acquires a magnetic moment.

Au is magnetic in various configurations, e.g. at interfaces where magnetism is attributed to holes in the d -band [28], but this mechanism is unlikely to occur here where the Au d -levels lie several eV in the valence band. S -electron magnetism has been predicted in bare Au clusters [29], that may be particularly stable in 2D [30]. Experimentally magnetism is observed in bare Au nanoclusters and ascribed to large spin-orbit coupling and reduced coordination at surfaces [31]. We observe negative MR in the as fabricated samples, when Au is clustered, which is enhanced on annealing suggesting the same mechanism may apply to moment formation here (supplementary information). The moment size cannot be independently extracted, but assuming it is $\sim 0.1 \mu_B$ implies that the graphene-Au exchange coupling is $O(\text{eV})$, comparable to dilute magnetic semiconductors [4].

Fig. 4b shows ρ_{xy} measured at hole and electron densities. After subtracting a linear term for the normal Hall effect contribution to obtain $\delta\rho_{xy} = \rho_{xy} - R_H B$ we observe sharp kinks that are largest at hole density, reaching approximately 90Ω at $N = -1 \times 10^{12} \text{ cm}^{-2}$. These features are reproduced between forward and reverse sweeps (red curve) without hysteresis, we attribute these to the anomalous Hall effect (AHE).

The AHE arises from either intrinsic or extrinsic mechanisms. The extrinsic AHE arises due to asymmetric scattering of electrons from local moments in the presence of spin orbit coupling. In Fig. 4d we show that the application of $B_{||}$ decreases the AHE contribution. The decrease in the AHE under $B_{||}$ contrasts with the enhancement of negative MR by $B_{||}$ (Fig. 3b); the decrease in $\delta\rho_{xy}$ when spin flip scattering is enhanced indicates an intrinsic origin of the AHE. This AHE survives close to room temperature.

Further work is required to characterize the magnetic behavior, but we speculate the AHE may occur due to chiral or topological magnetic defects that tend to be favored by the Dzyaloshinskii-Moriya interaction when inversion symmetry is broken, such as here. We note the similarity of the transport signatures observed here and those in topological magnetic phases such as MnSi under pressure [32] and magnetic topological insulators [33].

Finally we return to the large in-plane field effect on the electronic structure that is most pronounced at low density, close to the single band regime. Spin splitting in graphene occurs due to spin dependent hybridization with Au d -orbitals; this spin-orbit coupling also drives the formation of local moments implying these phenomena are strongly coupled. Close to the single band regime, where signatures of collective magnetism appear, the in-plane susceptibility of the electron gas is strongly enhanced [34]. This is likely to influence the magnetic state of the Au ions and thereby the spin splitting of graphene. This effect may also be related to magnetoelectric effects proposed by Zhang et al. [6].

To summarize we have demonstrated electronic hybridization between graphene and Au in an intercalated

graphene/hBN heterostructure. The observation of spin split LLs and the electric field effect demonstrates a Rashba interaction of approximately 25 meV, while negative MR and a large AHE suggest the proximity to a collective magnetic phase. Our results show that graphene hybridized with Au may be a platform for the electric field control of interactions between magnetic moments, and could satisfy the proposed requirements to create topological magnetic phases [6]. Further work is required to fully elucidate the magnetic interactions and enhance the size of these effects with other intercalation species.

We thank A.H. Castro-Neto, M. Cazalilla, A.R. Hamilton, T. Rappoport and I. Sodemann for fruitful discussions and S. Natarajan for assistance. This work was supported by the NRF, Prime Ministers Office, Singapore, under its Competitive Research Programme (CRP award number NRF-CRP9-2011-3), the SMF-NUS Research Horizons Award 2009-Phase II and the NRF, Prime Minister Office, Singapore, under its Medium-Sized Centre Programme.

* ectof@icloud.com

† barbaros@nus.edu.sg

- [1] C. Weeks, J. Hu, J. Alicea, M. Franz, and R. Wu, *Physical Review X* **1**, 021001 (2011).
- [2] D. Marchenko, A. Varykhalov, M. Scholz, G. Bihlmayer, E. Rashba, A. Rybkin, A. Shikin, and O. Rader, *Nature Communications* **3**, 1232 (2012).
- [3] F. Calleja, H. Ochoa, M. Garnica, S. Barja, J. J. Navarro, A. Black, M. M. Otrokov, E. V. Chulkov, A. Arnau, A. L. Vázquez de Parga, *et al.*, *Nature Physics* **11**, 43 (2015).
- [4] T. Dietl and H. Ohno, *Reviews of Modern Physics* **86**, 187 (2014).
- [5] Z. Qiao, S. A. Yang, W. Feng, W.-K. Tse, J. Ding, Y. Yao, J. Wang, and Q. Niu, *Physical Review B* **82**, 161414 (2010).
- [6] H. Zhang, C. Lazo, S. Blügel, S. Heinze, and Y. Mokrousov, *Physical Review Letters* **108**, 056802 (2012).
- [7] C. Dean, A. Young, I. Meric, C. Lee, L. Wang, S. Sorgenfrei, K. Watanabe, T. Taniguchi, P. Kim, K. Shepard, and J. Hone, *Nature Nanotechnology* **5**, 722 (2010).
- [8] J. M. Yuk, K. Kim, B. Alemán, W. Regan, J. H. Ryu, J. Park, P. Ercius, H. M. Lee, A. P. Alivisatos, M. F. Crommie, *et al.*, *Nano Letters* **11**, 3290 (2011).
- [9] L. Wang, I. Meric, P. Huang, Q. Gao, Y. Gao, H. Tran, T. Taniguchi, K. Watanabe, L. Campos, D. Muller, *et al.*, *Science* **342**, 614 (2013).
- [10] I. Gierz, T. Suzuki, R. T. Weitz, D. S. Lee, B. Krauss, C. Riedl, U. Starke, H. Höchst, J. H. Smet, C. R. Ast, *et al.*, *Physical Review B* **81**, 235408 (2010).
- [11] Y. Wu, W. Jiang, Y. Ren, W. Cai, W. H. Lee, H. Li, R. D. Piner, C. W. Pope, Y. Hao, H. Ji, *et al.*, *Small* **8**, 3129 (2012).
- [12] Z. Jia, R. Zhang, Q. Han, Q. Yan, R. Zhu, D. Yu, and X. Wu, *Applied Physics Letters* **105**, 143103 (2014).
- [13] A. Ferreira, T. G. Rappoport, M. A. Cazalilla, and A. H. Castro Neto, *Physical Review Letters* **112**, 066601 (2014).
- [14] J. Balakrishnan, G. K. W. Koon, A. Avsar, Y. Ho, J. H. Lee, M. Jaiswal, S.-J. Baeck, J.-H. Ahn, A. Ferreira, M. A. Cazalilla, *et al.*, *Nature Communications* **5**, 4748 (2014).
- [15] T. Hayashi, Y. Hashimoto, S. Katsumoto, and Y. Iye, *Applied Physics Letters* **78**, 1691 (2001).
- [16] A.-P. Li, C. Zeng, K. van Benthem, M. F. Chisholm, J. Shen, S. N. Rao, S. Dixit, L. C. Feldman, A. G. Petukhov, M. Foygel, *et al.*, *Physical Review B* **75**, 201201 (2007).
- [17] A. Barreiro, R. Rurli, E. R. Hernández, and A. Bachtold, *Small* **7**, 775 (2011).
- [18] T. Taychatanapat, K. Watanabe, T. Taniguchi, and P. Jarillo-Herrero, *Nature Physics* **7**, 621 (2011).
- [19] E. I. Rashba, *Physical Review B* **79**, 161409 (2009).
- [20] K. K. Choi, B. F. Levine, N. Jarosik, J. Walker, and R. Malik, *Physical Review B* **38**, 12362 (1988).
- [21] F. Qu, A. J. A. Beukman, S. Nadj-Perge, M. Wimmer, B.-M. Nguyen, W. Yi, J. Thorp, M. Sokolich, A. A. Kiselev, M. J. Manfra, C. M. Marcus, and L. P. Kouwenhoven, *Physical Review Letters* **115**, 036803 (2015).
- [22] M. Diez, A. M. R. V. L. Monteiro, G. Mattoni, E. Cobanera, T. Hyart, E. Mulazimoglu, N. Bovenzi, C. W. J. Beenakker, and A. D. Caviglia, *Physical Review Letters* **115**, 016803 (2015).
- [23] E. V. Kurganova, H. J. van Elferen, A. McCollam, L. A. Ponomarenko, K. S. Novoselov, A. Veligura, B. J. van Wees, J. C. Maan, and U. Zeitler, *Physical Review B* **84**, 121407 (2011).
- [24] I. Sodemann, Private communication (2015).
- [25] H. Min, J. E. Hill, N. A. Sinitsyn, B. R. Sahu, L. Kleinman, and A. H. MacDonald, *Physical Review B* **74**, 165310 (2006).
- [26] S. Abdelouahed, A. Ernst, J. Henk, I. V. Maznichenko, and I. Mertig, *Physical Review B* **82**, 125424 (2010).
- [27] R. Khosla and J. Fischer, *Physical Review B* **2**, 4084 (1970).
- [28] F. Wilhelm, M. Angelakeris, N. Jaouen, P. Pouloupoulos, E. T. Papaioannou, C. Mueller, P. Fumagalli, A. Rogalev, and N. K. Flevaris, *Physical Review B* **69**, 220404 (2004).
- [29] W. Luo, S. Pennycook, and S. Pantelides, *Nano letters* **7**, 3134 (2007).
- [30] Y. C. Choi, W. Y. Kim, H. M. Lee, and K. S. Kim, *Journal of Chemical Theory and Computation* **5**, 1216 (2009).
- [31] V. Tuboltsev, A. Savin, A. Pirojenko, and J. Räisänen, *ACS nano* **7**, 6691 (2013).
- [32] R. Ritz, M. Halder, M. Wagner, C. Franz, A. Bauer, and C. Pfleiderer, *Nature* **497**, 231 (2013).
- [33] K. Yasuda, R. Wakatsuki, T. Morimoto, R. Yoshimi, A. Tsukazaki, K. S. Takahashi, M. Ezawa, M. Kawasaki, N. Nagaosa, and Y. Tokura, *Nature Physics* **12**, 555 (2016).
- [34] R. A. Žak, D. L. Maslov, and D. Loss, *Physical Review B* **82**, 115415 (2010).